Nuclear Engineering and Technology 49 (2017) 576–580

Available online at ScienceDirect

Nuclear Engineering and Technology

journal homepage: www.elsevier.com/locate/net

Original Article

Application of a Dynamic-Nanoindentation Method to Analyze the Local Structure of an Fe-18 at.% Gd Cast Alloy

Yong Choi [a], *Youl Baik* [a], *Byung M. Moon* [b], *and Dong-Seong Sohn* [c,*]

[a] *Department of Materials Science and Technology, Dankook University, 119 Dandae-ro, Dongnam-gu, Cheonan, Chungnam 31116, South Korea*

[b] *Liquid Processing and Casting Technology R and D Group, KITECH, 156 Gaetbeol-ro, Yeonsu-gu, Incheon, 21999, South Korea*

[c] *Nuclear Engineering Department, UNIST, 50 UNIST-gil, Eonyang-eup, Ulju-gun, Ulsan, 689-798, South Korea*

ARTICLE INFO

Article history:
Received 11 February 2016
Received in revised form
3 September 2016
Accepted 3 October 2016
Available online 24 October 2016

Keywords:
Fe-Gd Cast Alloy
Nano-indentation
Neutron-absorbing Materials

ABSTRACT

A dynamic nanoindentation method was applied to study an Fe-18 at.% Gd alloy as a neutron-absorbing material prepared by vacuum arc-melting and cast in a mold. The Fe-18 at.% Gd cast alloy had a microstructure with matrix phases and an Fe-rich primary dendrite of Fe_9Gd. Rietveld refinement of the X-ray spectra showed that the Fe-18 at.% Gd cast alloy consisted of 35.84 at.% Fe_3Gd, 6.58 at.% Fe_5Gd, 16.22 at.% Fe_9Gd, 1.87 at.% Fe_2Gd, and 39.49 at.% β-$Fe_{17}Gd_2$. The average nanohardness of the primary dendrite phase and the matrix phases were 8.7 GPa and 9.3 GPa, respectively. The fatigue limit of the matrix phase was approximately 37% higher than that of the primary dendrite phase. The dynamic nanoindentation method is useful for identifying local phases and for analyzing local mechanical properties.

1. Introduction

The development of better neutron-absorbing materials is one of the greater necessities in the nuclear industry owing to the expected demand for spent nuclear fuel transportation and storage [1–3]. Due to the high neutron absorption cross-sections of boron and gadolinium, alloys containing boron and/or gadolinium in the form of BORAL, METAMIC, or borated stainless steel have been used as neutron-absorbing materials [4]. Given that boron produces helium gas as it absorbs neutrons, gadolinium-containing alloys are under development as neutron-absorbing structural materials [5,6]. Compared with boron, gadolinium has several advantages, such as a much higher thermal neutron-absorption cross-section (more than 60 times higher for Gd-157 than for B-10) and a higher isotopic abundance of a strong neutron absorber at 30.45% (Gd-155, Gd-157) versus 19.9% (B-10) [2–6]. From the perspective of irradiation performance, Gd remains as Gd as it absorbs a neutron (only the mass number increases), while boron produces a gas.

From a metallurgical standpoint, the melting and casting process used to obtain gadolinium-containing alloys cause

* *Corresponding author.*
E-mail address: dssohn@unist.ac.kr (D.-S. Sohn).
http://dx.doi.org/10.1016/j.net.2016.10.002

difficulties in producing an alloy with a homogeneous distribution and in the selection of a crucible due to its high oxidation affinity [1,6]. One of the methods used to mitigate these issues is to re-melt several mother alloys. Various mother alloys were prepared by a precise vacuum melting process involving a high concentration of Gd; these are then diluted to obtain the required composition by re-melting. One of the mother alloys was 18 at.% of Gd in Fe, which was selected based on the Fe-Gd binary phase diagram and suitable cast conditions.

Because the Fe-Gd mother alloy has a cast microstructure, it is necessary to develop a reliable and convenient method to determine the gadolinium distribution on the submicron scale because gadolinium as a rare-earth element cannot easily be analyzed by conventional techniques using X-rays and electron beams [7]. Among the various tools used to analyze a local area, the nanoindenter is very useful in materials science and engineering fields owing to its quantitative capabilities, conventional, and economic factors [8]. Although nondestructive analysis methods using ultrasonic waves, X-rays, and neutron scattering provide local chemical information, they cannot precisely evaluate physical and mechanical values [9]. Recently, a dynamic indentation method using a tribo-nanoindenter received attention due to its capability to evaluate various mechanical properties such as the nanohardness, friction coefficient, and fatigue limit of a material. Although the dynamic nanoindentation method has the ability to measure various mechanical properties of brittle materials such as ceramics, irradiated alloys, and intermetallics, little information has been achieved thus far, especially in relation to metallic phases [10–12]. Hence, we apply the method to an analysis of a Fe-Gd alloy, especially to determine the mechanical properties of the local phase of the alloy.

2. Materials and methods

The Fe-18 at.% Gd alloys were plasma vacuum arc-melted (PAM-Plasma, Miyoshi-shi, Japan) with iron (Fe > 99.9%, BASEF, Seoul, Korea) and gadolinium metal slots (Gd > 99.9%, HBVAM, Suzhou, China). The microstructure was observed by scanning electron microscopy (JSM 6400, Jeol, Tokyo, Japan). A chemical analysis and phase identification were carried out by electron microprobe analysis (JXA-8500F, Jeol, Japan) and X-ray diffractometry (Rigaku, Tokyo, Japan), respectively. The dynamic nanohardness of each phase of the alloys was determined with a tribo-nanoindenter (Hysitron, TI 750, Minneapolis, USA).

3. Results and discussion

3.1. *Microstructural observation and phase identification*

Fig. 1 shows the typical microstructure of the Fe-18 at.% Gd cast alloy. As shown in Fig. 2, two regions of the Fe-18 at.% Gd alloy were clearly observed with different levels of contrast. One is the primary dendrite and the other is the matrix. Considering a Fe-Gd binary phase diagram, the plausible phase of the primary dendrite phase in the Fe-18 at.% Gd alloy is Fe_9Gd, and different types of intermetallic phases are present because the low solubility of Gd in Fe causes the segregation of the Gd during cooling.

In order to determine the Gd distribution of the alloy, an electron microprobe analysis was carried out. Fig. 2 shows the Fe and Gd distribution as determined by the electron microprobe analysis. As shown in Fig. 2, the dark and blue regions are Fe-rich and Gd-rich phases, respectively. This finding supports the contention that Gd was segregated and present, therefore, as various phases.

Fig. 3 shows typical X-ray spectra of the vacuum arc-melted Fe-18 at.% Gd alloy for a qualitative identification of the phases. Table 1 presents the results of the Rietveld refinement ($\chi^2 = 6.24$) of the X-ray spectra to determine the phases quantitatively. As shown in Fig. 3 and Table 1, the Fe-18 at.% Gd alloy prepared by vacuum arc-melting is composed of 35.84 at.% Fe_3Gd ($R\bar{3}$ m), 6.58 at.% Fe_5Gd (P6/mmm), 1.87 at.% Fe_2Gd (Fd3m), 16.22 at.% Fe_9Gd ($R\bar{3}$ m) and 39.49 at.% β-$Fe_{17}Gd_2$ (P63/mmc). Because the primary dendrite with the Fe-rich composition was initially formed during the solidification step, the two regions of the Fe-18 at.% Gd alloy shown in Fig. 1 were such that the primary dendrite (as region-A) was Fe_9Gd ($R\bar{3}$ m), which becomes β-$Fe_{17}Gd_2$, and the matrix (as region-B) consisted of other intermetallics such as Fe_3Gd and Fe_5Gd, which formed later.

3.2. *Nanomechanical properties*

Because two regions with different morphologies were clearly present, as shown in the microstructure in Fig. 1, and the cast alloy was too brittle to be machined to a standard tensile test specimen, dynamic nanoindentation tests of regions A and B were carried out to determine the local mechanical properties of each phase in this study. The average nanohardness values for regions A and B were 8.7 GPa and 9.3 GPa, respectively, indicating that the primary phase of region A in Fig. 1 is softer than the primary phase of region B.

It is interesting to determine additional mechanical properties of the primary dendrite and the matrix which are regions A and B in Fig. 1. In this study, a modified Alekhin model

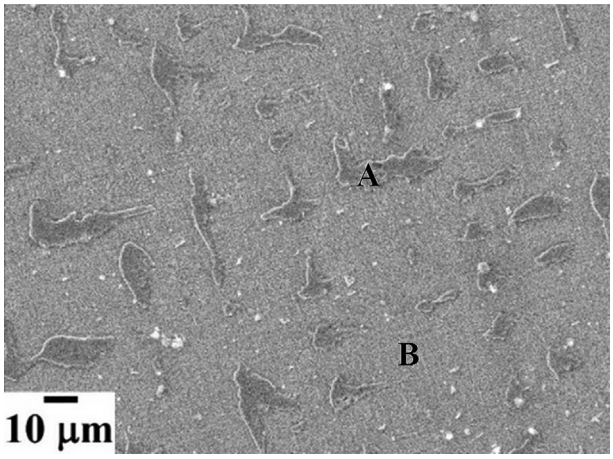

Fig. 1 – Scanning electron microscopy (SEM) image of Fe-18 at.% Gd alloy prepared by vacuum arc-melting. (A) primary dendrite. (B) matrix.

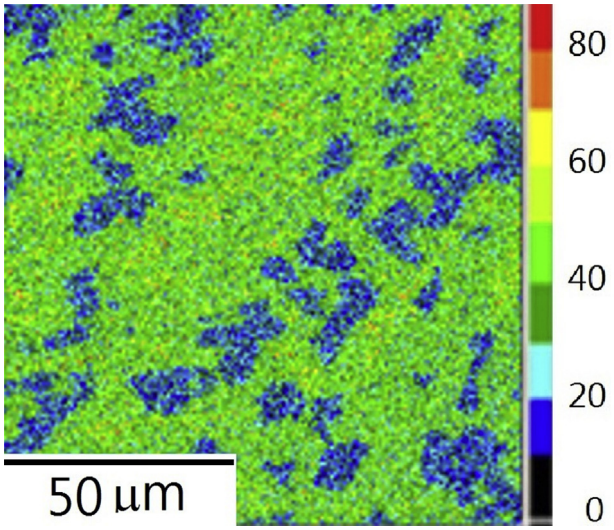

Fig. 2 – Gd-distribution of Fe-18 at.% Gd cast alloy analyzed by electron microprobe analysis (EMPA).

was applied to determine the fatigue limits of the local phases [13–16]. Because the nanohardness depends on various metallurgical factors on the surface, such as the residual stress, crystallographic structure, and defects, the local mechanical properties on the surface were determined by a nanohardness test. Repeating loading at a point can determine the local plastic deformation and strain hardening behaviors, which are related to fatigue limits. The fatigue limit of a local area on the nanoscale depends significantly on the local plastic deformation and on strain hardening behaviors such as dislocation moving, the slip system, and the Peierls-Nabarro stress. The geometry of a dent formed by nanoindenting is described by the indentation geometry, such as the dent width and depth. When the indenter tip creates the indenter width (W) on the surface of a specimen, elastic and plastic deformations occur. Because elastic relaxation occurs, the actual dent depth (δ) caused by plastic deformation produces local residual stain (ε). The plastic strain can be described by the nonlinear Hooke's law with an exponential function with a strain-hardening effect. The local residual

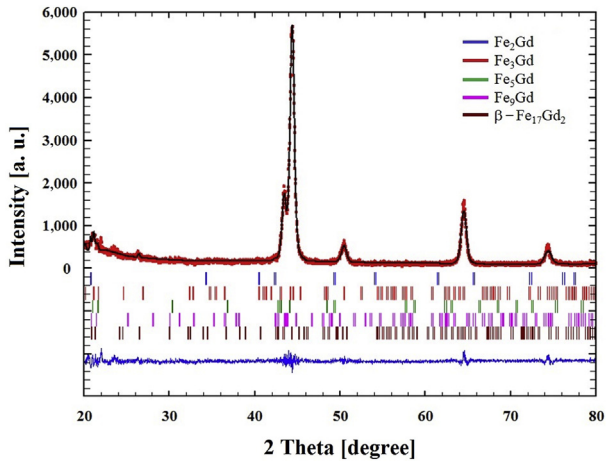

Fig. 3 – X-ray spectra of Fe-18 at.% Gd alloy prepared by vacuum arc-melting.

strain is exponentially proportional to (δ/W), as in Eq. (1) with the strain-hardening effect, where n is a constant denoting the strain-hardening effect:

$$\varepsilon = \kappa\left(\frac{\delta}{W_f}\right)^n \tag{1}$$

The final indenter width (W_f) after repeated or cyclic loading at a local area becomes infinite under the condition of nonresidual plastic deformation, such as an extremely brittle surface condition. The constant (n) for the strain-hardening effect is assumed to have a value identical to that of the empirical strain-hardening factor (n) of the alloys, which is usually in the range of 0.134 to 0.23 [8].

For a relatively minor amount of plastic deformation on the surface, the macroscopic indenter width of (W_L) is expressed by Eq. (2) with the tip angle (ϕ) and an indentation geometric value such as the radius (R):

$$W_L = \frac{2R_{max}}{1-\sin\phi} \tag{2}$$

Because limited strain hardening by repeating or cyclic loading with the same tip geometry at a local area causes the local surface to reach the condition of nonresidual plastic deformation, Eq. (3) is derived From Eqs. (1) and (2) because the maximum stain (ε_{max}) after repeated and cyclic loading at the same local area is such that the final indenter width (W_f) reaches the final maximum value of (W_L):

$$\frac{\varepsilon}{\varepsilon_{max}} = \left(\frac{\delta}{\delta_{max}}\right)^n \tag{3}$$

The Alekhin model suggested that the fatigue behavior depended on the surface force of the materials when the nanoindenter tip reached the yield point. Because the surface force is related to the indenter depth and width, the cyclic loading is explained by the indenter depth divided by the indenter width, indicating that the ratio of deformation geometry after the repeated loading by the nanoindentation can determine the fatigue limit value, because the fatigue limit is related to the accumulated plastic deformation.

Fig. 4 shows the cycling load-deflection curves of local regions A and B in Fig. 1 as determined by tribo-nanoindentation. As shown in Figs. 4A and 4B, the four steps of loading, creep, unloading, and recovery were clearly observed to be related to the material behavior under the condition studied here. The loading step is the indenting step with an increase in the load, the creep step is the deformation step at the maximum load, the unloading step is the stress relaxation step, and the recovery step is the strain relaxation step. The main difference between Fig. 4A and 4B is the load for the initiation of stress relaxation of the primary phase; the value for region A was lower than 1.0 mN, whereas that of the matrix phase was approximately 1.8 mN. Furthermore, the final load for strain relaxation of the primary phase was close to 0.3 mN, whereas that of the matrix phase was 1.4 mN. This indicates that the primary phase is softer and more elastically deformed with less of a strain-hardening effect than the matrix for a given load.

Fig. 5 shows the repeated loading-volume strain curves, which can be used to estimate the fatigue behavior of the

Table 1 – Rietveld refinement of Fe-18 at.% Gd alloy prepared by vacuum arc-melting ($\chi^2 = 6.24$).

Phase	Fe_2Gd	Fe_3Gd	Fe_5Gd	Fe_9Gd	β-$Fe_{17}Gd_2$
Content (at.%)	1.87 (1)	35.84 (2)	6.58 (2)	16.22 (2)	39.49 (2)
Lattice parameter					
a (Å)	7.39378 (268)	5.16482 (68)	4.88205 (1872)	8.52920 (154)	8.50372 (71)
b (Å)	7.39378 (268)	5.16482 (68)	4.88205 (1872)	8.52920 (154)	8.50372 (71)
c (Å)	7.39378 (268)	24.61737 (1324)	4.11167 (124)	12.45231 (355)	8.34421 (122)
α (degree)	90	90	90	90	90
β (degree)	90	90	90	90	90
γ (degree)	90	120	120	120	120

primary phase and the matrix as determined by the dynamic indentation method using the Alekhin model. There are two segments of the curve: the initial slope for strain hardening by repeated loading and the saturated volume strain for fatigue limits. As shown in Fig. 5, the primary phase has a lower fatigue limit, which is related to the ductility of the primary phase as observed using the dynamic nanoindentation method in Fig. 4. Because the ratio of the indenter depth (δ_i) and the indenter width (W_i) for repeated loading reachs a certain value, the value (δ/W_i) becomes the fatigue limit.

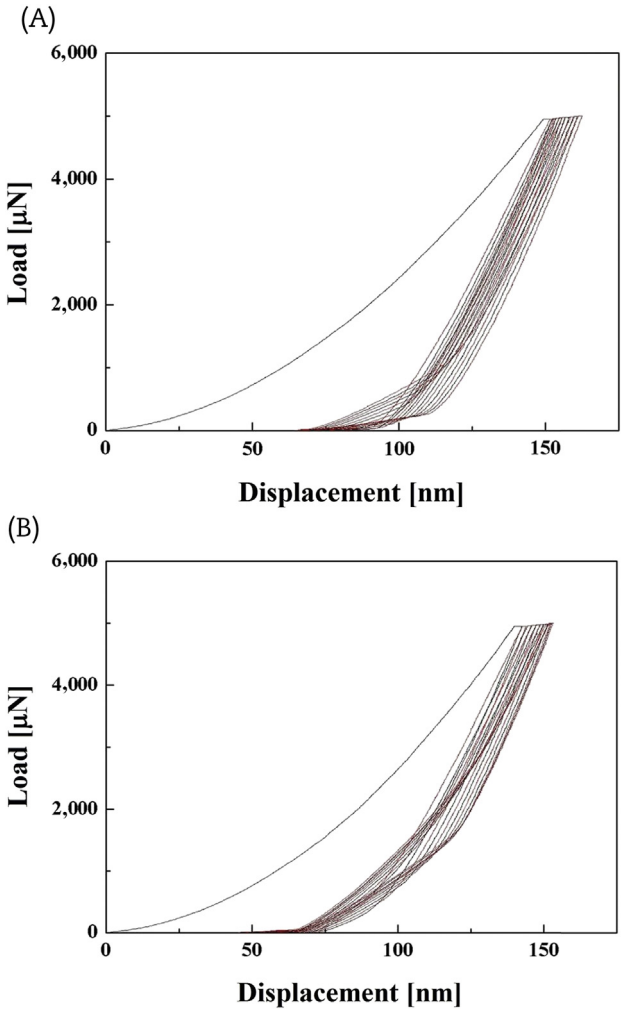

Fig. 4 – Typical load-depth-displacement curves of Fe-18 at.% Gd alloy. (A) the primary dendrite phase. (B) the matrix.

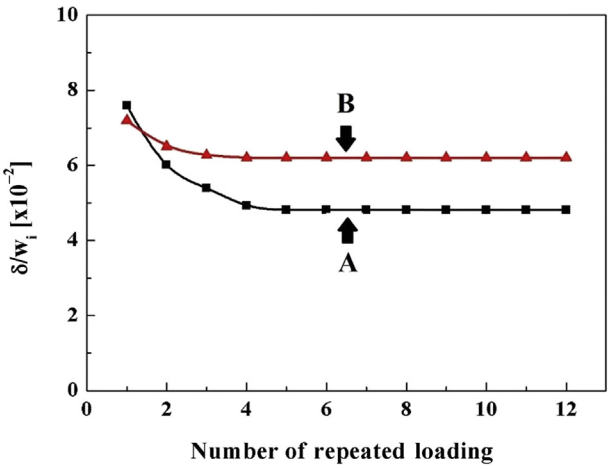

Fig. 5 – Fatigue limit of local intermetallic phases of Fe-18 at.% Gd alloy prepared by vacuum arc-melting. (A) primary dendrite region- A of Fig. 1. (B) matrix region-B of Fig. 1.

Although the fatigue limit proposed by the Alekhin model does not indicate the type of cyclic loading, such as the high cycle and low cycle of a conventional macro-fatigue test of metallic phases, it appears to be possible to determine the relative fatigue life of the phase at the nanoscale. In this study, the fatigue limits of the primary phase and the matrix were close to 4.6 and 6.3, respectively, indicating that the fatigue limit of the matrix phase is nearly 37% higher than that of the primary dendrite phase. Hence, the primary dendrite phase is $Fe_9Gd(R\bar{3}\ m)$, which becomes β-$Fe_{17}Gd_2$(P63/mmc). It is relatively soft and has a low fatigue limit. The matrix has mainly two phases, Fe_3Gd ($R\bar{3}\ m$) and Fe_5Gd (P6/mmm) with a small amount of Fe_2Gd (Fd3m), which is relatively hard and has a high fatigue limit. From these results, it can be concluded that the dynamic nano-indentation method is useful for phase identification and for studying the mechanical properties of local phases.

4. Conclusions

Fe-18 at.% Gd alloys were well produced by vacuum arc-melting and casting processes for a mother alloy of Gd-containing stainless steels which can be used as neutron-absorbing materials. The Fe-18 at.% Gd cast alloy had a dendrite structure. The primary dendrite was a high Fe-rich phase, in this case Fe_9Gd, and it became β-$Fe_{17}Gd_2$. The

matrix mainly consisted of the two phases of Fe_3Gd and Fe_5Gd with a small amount of Fe_2Gd. Rietveld refinement showed that the cast alloy of Fe-18 at.% Gd consists of 35.84 (2) at.% Fe_3Gd, 6.58 (2) at.% Fe_5Gd, 16.22 (2) at.% Fe_9Gd, 1.87 (1) at.% Fe_2Gd, and 39.49 (2) at.% β-$Fe_{17}Gd_2$. The average nanohardness of the primary dendrite phase of Fe_9Gd and the matrix phases as determined by nanohardness testing were 8.7 GPa and 9.3 GPa, respectively. The fatigue limit of the matrix phases is approximately 37% higher than that of the primary dendrite phase. The dynamic nanoindentation method is useful for identifying local phases and for analyzing local mechanical properties.

Conflicts of interest

All contributing authors declare no conflicts of interest.

Acknowledgments

This work was supported by the Nuclear Power Core Technology Development Program of the Korea Institute of Energy Technology Evaluation and Planning (KETEP), granted financial resource from the Ministry of Trade, Industry & Energy, Republic of Korea. (No. 20131520000060)

REFERENCES

[1] Y. Choi, Y. Baik, B.M. Moon, D.-S. Sohn, Fabrication of Gd containing duplex stainless steel sheet for neutron absorbing structural materials, Nucl. Eng. Technol. 25 (2013) 689–691.
[2] Y. Choi, B.M. Moon, D.-S. Sohn, Corrosion and wear properties of cold rolled 0.087% Gd lean duplex stainless steels for neutron absorbing material, Nucl. Eng. Technol. 48 (2016) 164–168.
[3] D.-Y. Kim, S.G. Hong, G.H. Ahn, iBEST: a program for burnup history estimation of spent fuels based on ORIGEN-S, Nucl. Eng. Technol. 47 (2015) 596–607.
[4] A. Machiels, R. Lambert, Handbook of Neutron Absorber Materials for Spent Nuclear Fuel Transportation and Storage Applications, 2009-ed., Electronic Power Research Institute, Palo Alto, CA, 2009. EPRI-RR-1019110.
[5] G.W. Wachs, J.W. Sterbentz, L.M. Montierth, F.K. Tovesson, T.S. Hill, Characterization of an Advanced Gadolinium Neutron Absorber Alloy by Means of Neutron Transmission, INL/CON-07–12838, Idaho National Laboratory, Idaho Falls, ID, 2007.
[6] G.W. Wachs, J.W. Sterbentz, Nickel Based Gadolinium Alloy for Neutron Adsorption Application in Ram Package, PATRAM 2007, Miami, Florida, Oct. 2007.
[7] S.B. Oh, Y. Choi, H.G. Jung, S.W. Kho, C.S. Lee, Non-destructive analysis of hydrogen-induced cracking of API steels using acoustic microscopy and small-angle neutron scattering, Phys. Met. Metallogr. 115 (2014) 1366–1370.
[8] V.P. Alekhin, I.S. Cho, Y.S. Pyun, Y.H. Kang, Y. Choi, Application of nano-indentation method to statically evaluate irradiated materials, in: Proceedings of Korea Surface Engineering Society Spring Meeting, Seoul, May, 2003.
[9] M.S. Song, Y. Choi, K.N. Choo, D.S. Kim, Y.H. Kang, Evaluation of mechanical properties of irradiated materials by nano-indentation technique, in: Proceedings of International Symposium on Research Reactor and Neutron Science, Daejeon, Korea, April, 2005.
[10] Y. Choi, Irradiation Effect on the Phase Transformations and Corrosion Behavior of Nano-structured Composites, KAERI/RR, Korea Atomic Energy Institute, 2004.
[11] K.S. Choi, Y. Choi, B.G. Kim, Y.W. Lee, Evaluation of friction coefficient and compressive strength of graphite layers of nuclear fuel for HGTR by kinetic nano-indentation technique, in: Proceeding of Annual Korean Nuclear Society Fall Meeting, Kyungju, Korea, November, 2006.
[12] K.S. Choi, Y. Choi, B.G. Kim, Y.W. Lee, Evaluation of mechanical properties of graphite layers on a nuclear fuel particle by kinetic nano-indentation technique, Key Eng. Mater. 345–346 (2007) 1177–1180.
[13] W.C. Oliver, G.M. Pharr, An improved technique for determining hardness and elastic-modulus using load and displacement sensing indentation experiments, J. Mater. Res. 7 (1992) 1564–1583.
[14] S.I. Bulychev, V.P. Alekhin, M.K. Shorshorov, A.P. Ternovskii, G.D. Shnyrev, Determination of Young's modulus according to indentation diagram, Zavod. Lab. 41 (1975) 1137–1141.
[15] V.P. Alekhin, S.I. Bulychyov, E.Y. Lyapunova, Structure of materials and statistical characteristics of indentation, J. Tambov State University 3 (1998) 1–98.
[16] P. Ogar, D. Gorokhov, Meyer law application for solving problems of surface plastic deformation by spherical indentation, Appl. Mech. Mater. 788 (2015) 199–204.